The Effect of Backbone Rigidity on the Glass Transition of Polymers of Intrinsic Microporosity Probed by Fast Scanning Calorimetry

Huajie Yin*+, Bin Yang‡, Yeong Zen Chua‡, Paulina Szymoniak+, Mariolino Cartax, Richard Malpass-Evans#, Neil B. McKeown#, Wayne J. Harrison§, Peter M. Budd§, Christoph Schick‡, Martin Böhning+, Andreas Schönhals*+

+ Bundesanstalt für Materialforschung und –prüfung (BAM), Unter den Eichen 87, 12205 Berlin, Germany

‡ University of Rostock, Institute of Physics and Competence Center CALOR, Albert-Einstein-Str. 23–24, 18059 Rostock, Germany

x Department of Chemistry, College of Science. Swansea University, Singleton Park, Swansea, Wales SA2 8PP, UK

EastChem, School of Chemistry, University of Edinburgh, David Brewster Road, Edinburgh EH9 3FJ, UK

§ School of Chemistry, University of Manchester, Manchester M13 9PL, UK

KEYWORDS Polymers of Intrinsic Microporosity, Membranes, Glass transition, Fast Scanning Calorimetry.

ABSTRACT: Polymers of Intrinsic Microporosity (PIMs) of high performance have developed as materials with a wide application range in gas separation and other energy-related fields. Further optimization and long-term behavior of devices with PIMs require an understanding of the structure-property relationships including physical aging. In this context the glass transition plays a central role, but with conventional thermal analysis a glass transition is usually not detectable for PIMs before their thermal decomposition. Fast scanning calorimetry provides evidence of the glass transition for a series of PIMs, as the time scales responsible for thermal degradation and for the glass transition are decoupled by employing ultrafast heating rates of tens of thousands K s^{-1}. The investigated PIMs were chosen considering the chain rigidity. The estimated glass transition temperatures follow the order of the rigidity of the backbone of the PIMs.

Polymers of Intrinsic Microporosity (PIMs) as microporous materials having interconnected pores of characteristic sizes less than 2 nm and Brunauer–Emmett–Teller (BET) surface areas mostly larger than 700 m^2 g^{-1}. Different from porous organic polymers (POPs) consisting of a three-dimensional covalent network of cross-linked repeating units, PIMs are composed of discrete macromolecular chains with a rigid and contorted backbone, leading to inefficient packing in the solid state.[1] PIMs are soluble in conventional solvents what enables their processing into robust films, coatings or fibers. Their unique structural features and properties make them suitable for devices such as organic light emitting diodes (OLEDs) and sensors,[2-4] and for the production of membranes[5] for gas separations,[6,7] pervaporation,[8,9] and nanofiltration.[10] Further applications in water treatment,[11-13] gas storage,[14-16] and electrochemical devices have also been suggested.[17-23]

In addition to the twisted chain structure of PIMs achieved by introducing sites of contortion, such as the spiro-centers of PIM-1,[5] they possess limited freedom of motion arising from prohibited rotation along the polymer backbone for instance via fused-ring structures. However, it would be misleading to assume that such rigid structures are completely incapable of small-scale rotational fluctuations. Computer simulations suggest that the chain-forming dioxane bridges and spirobisindane (SBI) linkages in PIM-1 (Figure 1, panel B) still flex considerably.[24] Dielectric measurements on PIM-1 films also provided evidence of a relaxation process related to local fluctuations.[25] In our recent work for the first time a glass transition in PIM-1 was observed applying fast scanning calorimetry (FSC).[26] Aiming a further enhancing of chain rigidity and insufficient packing – hence increasing the performance of PIMs in gas separations,[27] new structure designs were developed. For example, fusing ethanoanthracene (EA) and Tröger's base (TB) gave the highly rigid, irregularly shaped PIM-EA-TB[28,29] (Figure 1, panel A). PIM-EA-TB was confirmed to be more rigid than PIM-1 through modeling and this enhanced rigidity resulted in gas separation membranes with greater selectivity.[7] Nevertheless, partial collapse of the microporous structure induced by physical aging is commonly observed for all PIMs.[30,31]

Investigations of the glassy dynamics and its role in the formation and persistence of microporosity in PIMs are of fundamental and technological importance and further experimental studies are required.[25,32,33] Following the previous investigations of PIM-1 by FSC,[26] the present work extends this methodology to a series of polymers with a change in chain rigidity. In addition to the archetypal PIM-1, PIM-EA-TB and DMDPH-TB[34] were chosen (see Figure 1). The latter was considered to possess a more flexible chain than PIM-EA-TB or PIM-1 as it contains C-C single bonds within its methylene units.

Generally, the glass transition temperature (T_g) of polymers is the central parameter determining its behavior with respect to a wide range of applications. Below T_g, polymers are in a glassy state with solid-like elastic properties. Segmental motions are frozen. Physical aging, associated with local fluctuations, is closely related to the stability of end-use material properties

(volumetric, mechanical, electrical, gas permeability, etc.). Upon heating through T_g, polymers enter a rubbery state showing a distinct viscoelastic behavior. From a fundamental scientific perspective, the glass transition is an actual problem of condensed matter physics.

Generally, the T_g of a PIM is not detectable before thermal decomposition using conventional thermal methods like differential scanning calorimetry (DSC) and dynamic mechanical thermal analysis.[5,35] Recently, Fast Scanning Calorimetry was demonstrated to be a suitable method to prove the existence of a glass transition for PIM-1.[26] The strategy behind this approach is to decouple the time scales corresponding to the glass transition and to the thermal degradation by employing fast heating rates (tens of thousands K s^{-1}).[36]

The chemical structures of the investigated polymers are shown in Figure 1. Detailed information about their synthesis is given in the literature for PIM-EA-TB,[7] PIM-1,[5] and DMDPH-TB.[34] (see also Supporting Information). PIM-EA-TB consists entirely of benzene rings fused together by inflexible bridged bicyclic units. PIM-1 possesses a quite rigid repeating unit with a relatively flexible spiro-center as a site of contortion. DMDPH-TB consisted of TB units connected by a methylene unit (-CH_2-) about which the C-C single bonds allow in principle free rotation. Therefore, the overall rigidity of the polymer backbone is in the order of PIM-EA-TB>PIM-1> DMDPH-TB, as reflected in their apparent BET surface areas of 1050, 750 and 35 m^2 g^{-1}, respectively.[7] For conventional polymers, the glass transition is related to cooperative segmental fluctuations. In contrast, for most PIMs (e.g. PIM-EA-TB and PIM-1) with limited degrees of freedom, cooperative rearrangements of segments are excluded, and only local fluctuations are expected. Although DMDPH-TB with C-C bonds in each repeating unit might in principle allow for bond rotation, cooperative motions at the segmental level could only occur with difficulty, due to the rigid moiety containing a TB unit.

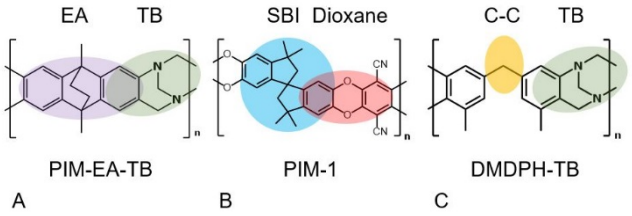

Figure 1. Chemical structures of three selected polymers. (A) PIM-EA-TB with EA (purple) and TB (green) units; (B) PIM-1 containing SBI (blue) and dioxane (red) linkages; (C) DMDPH-TB with C-C bond (yellow) and TB (green) unit.

The glass transition behavior of the polymers was investigated using a differential power-compensated fast scanning calorimeter based on the chip sensor XI-469 of Xensor Integration (Netherlands).[37,38] In the study of PIM-1, the sensor XI-415 was employed.[26] In short, the measurement principle is similar to the well-known power compensated differential scanning calorimetry, but the heaters and temperature sensors are integrated in the chip structure allowing for extreme high heating and cooling rates. Detailed information regarding the principle of the measurement and the setup are collected in the Supporting Information. For low sample masses and larger changes of the specific heat at T_g, heating and cooling rates of up to ~10^6 K s^{-1} can be achieved under optimized conditions. For the measurements, a small amount of a sample film was located on the sensor in the middle of the heated area and a thermal link between the sensor and the film was established by a spontaneous process. All reported measurements were conducted in air atmosphere, because no differences were found between measurements carried out in air and under protective argon atmosphere.

Results for PIM-1 have been reported earlier[26] and are included here for comparison with PIM-EA-TB and DMDPH-TB. The T_g of PIM-EA-TB was first roughly located between 600 K and 800 K by analyzing images of the sample after each heating run carried out by increasing the upper temperature limit stepwise. The pictures were taken using a microscope. (Figure S1 in the Supporting Information). After that procedure three complete heating/cooling experiments from 320 K to 850 K at a rate of 10^4 K s^{-1} was carried out. At this rate the duration of the heating interval is only ca. 0.05 s. In Figure 2A, these three successive heat flow curves for heating/cooling runs are depicted, which overlap each other, confirming the repeatability of the measurements and the absence of thermal decomposition. It proves also that essentially no significant amount of solvent is left in the sample from the preparation. (In reference 26 it was also shown that the FSC results are reproducible for different samples.) In both the heating and cooling cycles, a step in the heat flow was observed, which is generally considered as the characteristic feature of a glass transition in a DSC study. The mid-step height of the increment of the heat flow is used to estimate the glass transition temperature to be T_g = 663 K for PIM-EA-TB upon heating and cooling at a rate of 10^4 K s^{-1}. Consistent with the ladder-like rigid structure of PIM-EA-TB this value is high and, as expected, also higher than the T_g of PIM-1 (644 K) at the same heating rate (see below).[26] Pictures of the PIM-EA-TB film on the sensor surface were taken under a microscope after subsequent heating runs at 10^4 K s^{-1} (Figure S1 in the Supporting Information). Figures 2C and 2D display the effect when the glass transition region is crossed. Especially after heating to 850 K, i.e. above T_g, the sample became smaller and its edges more rounded. The observed shrinkage (see also Animation S1 in the Supporting Information) after the first heating to 850 K substantiates the occurrence of a glass transition leading to a significant softening of the sample and relaxation of internal stresses. In the following heating runs, only marginal changes in the size and form of the sample are observed because most of the stresses are relaxed during the first heating to 850 K. In contrast to that, the previous heating run to 700 K did not provide sufficient time above T_g (<<1 ms)) to allow for significant stress relaxation. It should be noted that even after ten complete heating/cooling experiments to 850 K with different heating/cooling rates no indications of a thermal degradation were detected. This was confirmed by FTIR measurements as reported in the previous work.[26] After these heating/cooling runs, the sample can be completely removed from the sensor by dissolving it. The solubility of the sample indicates that no cross-linking took place.

By employing data obtained from temperature-modulated DSC measurements on PIM-EA-TB (see Supporting Information Figure S7, S8), the heat flow data were converted

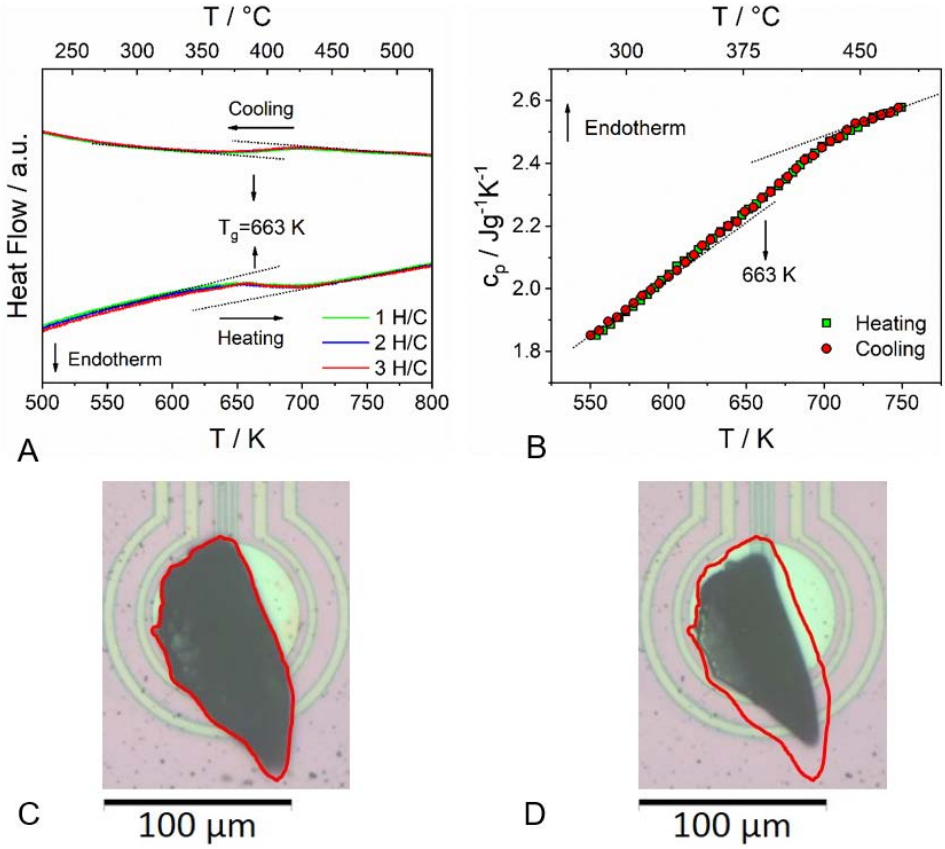

Figure 2. (A) Thermograms of PIM-EA-TB for 3 successive heating / cooling runs to 850 K with a rate of 10^4 K s^{-1}; (B) Specific heat capacity for the heating / cooling experiments estimated from FSC showing the glass transition; (C, D) Images of the PIM-EA-TB sample on the chip sensor obtained under a microscope at room temperature showing the effect of crossing the glass transition region. The red shape indicates the contour of the sample after heating to 700 K (C) compared to that after heating to 850 K (D). See Figure S1 in the Supplemental Information for the complete series of pictures.

into the specific heat capacity (c_p) as function of temperature as shown in Figure 2B. The c_p curve obtained from the heating run is in good agreement with the cooling run, which confirms the reliability of the experiment. Furthermore, from these data the sample mass could be calculated to be ca. 40 ng. A more detailed description of the data conversion and the sample mass calculation is given in the Supporting Information.

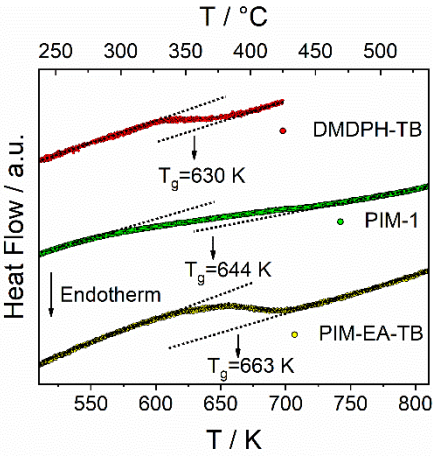

Figure 3. FSC curves obtained at a heating rate of 10^4 K s^{-1} for PIM-EA-TB, PIM-1 and DMDPH-TB. For clarity the curves were moved along the y-axis for clarity. The shape of the FSC curve measured for PIM-1 seems to be somewhat different than for the other two polymers. This is attributed to the fact that for the measurements of PIM-1 a slightly different sensor was employed.

In Figure 3 the heat flow curves for the three different PIMs at a heating rate of 10^4 K s^{-1} are compared. For PIM-EA-TB a T_g value of 663 K is found, which is 19 K higher than that of PIM-1 (T_g = 644 K)[26] and 33 K higher than that of DMDPH-TB (T_g = 630 K), consistent with the order of their expected backbone stiffness: PIM-EA-TB>PIM-1>DMDPH-TB. The scaling with the backbone rigidity is also observed for all other employed heating rates (see below). From the Analysis of the torsion angles of PIM-1 and PIM-EA-TB[7] a larger difference in T_g might be expected. In this respect it should be considered that the glass transition is not only due to intramolecular but also to intermolecular effects. Moreover, the glass transition temperature measured for DMDPH-TB is in a similar range than for the other both polymers with a rigid backbone structure. This result indicates that in the condensed state the chain flexibility of DMDPH-TB is not that large as it can be expected from the chemical structure.

According to the cooperativity approach the glass transition may be related to a length scale ξ[39] which can be roughly estimated in the framework of the fluctuation approach[40] to

$$\xi \approx \sqrt[3]{\frac{k_B T_g^2 \Delta\left(\frac{1}{c_P}\right)}{\rho(\delta T)^2}} \qquad (1)$$

where k_B is the Boltzmann constant, $\Delta(1/c_P)=1/c_{p,glass}-1/c_{p,liquid}$. Here $c_V \approx c_P$ is assumed, ρ is the density, and δT is the width of the glass transition. For conventional polymers δT is found to be ca. 10 to 20 K for comparable heating rates. For PIM-EA-TB the width of the glass transition is extremely large ($\delta T \approx 100$ K). Also, for PIM-1 and DMDPH-TB comparable values for δT were observed (see Table 1). The fact that the glass transition region is quite broad cannot be ascribed to a thermal lag due to the thickness of the sample (see Supporting Information). Moreover, the change of the specific heat capacity (c_P) at the glass transition is small, which indicates that only a limited number of degrees of freedom are involved in the glass transition. According to Equ. 1 ξ is estimated for all investigated polymers and given in Table 1 (for details see Supporting Information). For PIM-EA-TB the value of ξ is calculated to be 0.26 nm, which is much smaller compared to that of conventional polymers[41]. Since larger conformational changes can be ruled out as molecular origin of the glass transition in rigid PIMs, especially for PIM-EA-TB and PIM-1, small-scale flex and band rearrangements are most probably responsible for the observed glass transition of PIMs. These considerations are in agreement with the small values of ξ. Modes of local fluctuations are proposed here that are distinct from the other existing mechanisms responsible for glassy dynamics, i.e. rotational fluctuations, conformational transitions, or orientational changes as degrees of freedom.[40]

Table 1: Width δT, increment of the specific heat Δc_p, and length scale ξ at the glass transition. The data for PIM-1 are taken from ref. 26. For PIM-1 Δc_p was not estimated in ref. 26 for technical reasons.

	δT /K	Δc_p / J K^{-1}g^{-1}	ξ / nm
PIM-EA-TB	100	0.17	0.26
PIM-1	150		(0.22-0.29)
DMDPH-TB	80	0.16	0.29

Another characteristic feature of the glass transition is the distinct dependence of T_g on the heating rate.[42] Therefore, experiments with different heating rates β (from 10^4 K s^{-1} to 5×10^4 K s^{-1}) were conducted on PIM-EA-TB to test whether T_g shifts with increasing heating rates shifts to higher values. This is confirmed in Figure 4, showing that faster heating rates result in a higher T_g value similar to the behavior of PIM-1.[26]

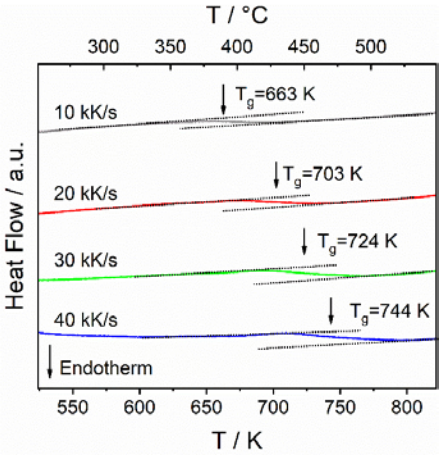

Figure 4. FSC curves of PIM-EA-TB obtained for successive heating experiments at indicated heating rates.

In Figure 5 the heating rate (β) is plotted as a function of inverse T_g in the so-called activation diagram. In general, a curved temperature dependence of the heating rate of the should be expected when plotted verus $1/T_g$ which should follow the Vogel-Fulcher-Tammann (VFT) equation.[43-46]

$$\beta(T_g) = B \exp\left(-\frac{DT_g^0}{T_g - T_g^0}\right) \qquad (2)$$

Here T_g^0 is the value of T_g in the limit of $\beta \to 0$. B is a fit parameter and has the dimension of a heating rate and D is the so-called fragility strength parameter. However, for the data of PIM-EA-TB in the limited range of heating rates a linear-like dependence versus 1/T is observed. If we approximate the data by an Arrhenius equation

$$\beta(T_g) = B \exp\left(\frac{-E_A}{k_B T_g}\right) \qquad (3)$$

the apparent activation energy (E_A) of the thermally activated process was estimated to be ca. 74 kJ/mol. This value is above the normal range of localized fluctuations in conventional polymers[47] (20−50 kJ mol^{-1}; In some cases, also higher activation energies have been reported for secondary processes, but these processes do not give rise to a calorimetric response.). The deduced value of activation energy is a rough estimation, as the error bars in the determined values of T_g of ±20 K are quite large and correspond to a broad range of activation energies from 53 kJ mol^{-1} to 130 kJ mol^{-1}. Considering this quite large error in the activation energy and the narrow range of rates (smaller than one decade) which could only be covered, it is most likely that for the observed behavior it could not be differentiated unambiguously between a VFT- and an Arrhenius-like temperature-dependence. It should be also noted that for the higher rates applied, the curvature of a VFT dependence becomes already smaller which impedes such a distinction and leads to a lower apparent activation energy. Nevertheless, in terms of the fragility approach to the glass transition it could not be excluded that the polymers considered here are behaving quite fragile leading to weaker temperature-dependence of heating rates than observed for conventional polymers. By relating the fast heating rates to short relaxation times this assignment is in agreement with the proposed more localized fluctuations responsible for the glass transition which are in between localized fluctuations

causing a β-relaxation and segmental motions related to α-relaxations in conventional, flexible polymers. Unfortunately, the study cannot be extended to lower hearting rates because the polymers will degrade when lower heating rates are applied. In Figure 5, data of PIM-1 and DMDPH-TB were included in the activation diagram. These data also support the conclusion that localized fluctuations are responsible for glassy dynamics in PIMs.

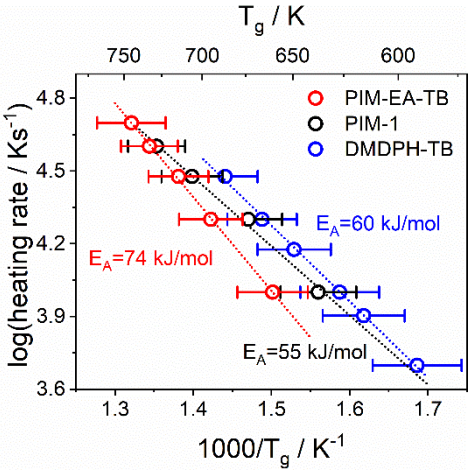

Figure 5. log(β) vs. inverse T_g for PIM-EA-TB, PIM-1, and DMDPH-TB. Error bars were calculated on the basis of ΔT_g = ±20 K for PIM-EA-TB, PIM-1 and DMDPH-TB. Data for PIM-1 were taken from reference 26.

In summary, the dependence of the glass transition of PIMs with a variation of the backbone rigidity has been clearly demonstrated by using FSC, where thermal decomposition was avoided by applying ultrafast heating rates (tens of thousands K s^{-1}). The glass transition temperatures (T_g) of the investigated PIMs were determined, i.e. PIM-EA-TB (663 K) > PIM-1 (644 K) > DMDPH-TB (630 K) for a value of the heating rate of 10^4 K s^{-1}, following the same order as their expected backbone rigidity. As conformational changes of the rigid chains are not possible, the glass transition is assigned to rather local, small-scale fluctuations. This is also true for DMDPH because the glass transition temperature is located in a similar temperature range than that of the PIMs. The results broaden the knowledge of the glassy dynamics of discrete rigid chains capable of forming permanently accessible microporosity and increase our understanding of the origin of the glass transition of this important new class of polymer. Physical aging of polymers is closely connected to molecular mobility and, hence, also to the glass transition. Based on the improved knowledge of the glass transition in the next step the physical aging of PIMs will be investigated in detail employing also FSC.[48-50]

ASSOCIATED CONTENT

Supporting Information.
The Supporting Information is available free of charge on the ACS Publications website at DOI: 10.1021/acsmacrolett.XXXXXXX.
Microscopic images, calculation of cooperative length scale, materials and sample preparation, experimental details about fast scanning calorimetry and temperature modulated differential scanning calorimetry, calculation of specific heat capacity and sample mass, animation showing shrinkage (PDF)

AUTHOR INFORMATION

Corresponding Author

* E-mail: huajie.yin@bam.de
andreas.schoenhals@bam.de

ORCID

Huajie Yin: 0000-0003-3949-5795
Bin Yang: 0000-0001-5534-9187
Yeong Zen Chua: 0000-0003-1375-3629
Paulina Szymoniak: 0000-0003-2152-5095
Mariolino Carta: 0000-0003-0718-6971
Richard Malpass-Evans: 0000-0002-6375-6273
Neil B. McKeown: 0000-0002-6027-261X
Wayne J. Harrison: 0000-0001-6253-1278
Peter M. Budd: 0000-0003-3606-1158
Christoph Schick: 0000-0001-6736-5491
Martin Böhning: 0000-0001-9753-345X
Andreas Schönhals: 0000-0003-4330-9107

Author Contributions

A.S. initiated the project. H.Y., B.Y., and Y.Z.C. conducted and analyzed the FSC measurements under supervision of C.S. P.S. conducted conventional and temperature modulated DSC measurements. W.J.H. and P.M.B. synthesized the PIM-1. M.C., RM. and N.McK. synthesized PIM-EA-TB and DMDPH-TB. H.Y., M.B. and A.S., guided the project and wrote the manuscript based on a first draft of H.Y. All authors discussed the results and commented on the manuscript.

Funding Sources

W. J. Harrison was supported by EPSRC grant EP/K016946/1 “Graphene-based membranes”.

Notes

The authors declare no competing financial interest.

ACKNOWLEDGMENT

The authors would like to thank G. Hidde for experimental help.

REFERENCES

(1) Dawson, R.; Cooper, A. I.; Adams, D. J. Nanoporous Organic Polymer Networks. *Prog. Polym. Sci.* **2012**, 37, 530-563.
(2) Gupta, B. K.; Kedawat, G.; Kumar, P.; Rafiee, M. A.; Tyagi, P.; Srivastava, R.; Ajayan, P. M. An n-type, New Emerging Luminescent Polybenzodioxane Polymer for Application in Solution-Processed Green Emitting OLEDs. *J. Mater. Chem. C* **2015**, 3, 2568-2574.
(3) Wang, Y.; McKeown, N. B.; Msayib, K. J.; Turnbull, G. A.; Samuel, I. D. W. Laser Chemosensor with Rapid Responsivity and Inherent Memory Based on a Polymer of Intrinsic Microporosity. *Sensors* **2011**, 11, 2478-2487.
(4) Rakow, N. A.; Wendland, M. S.; Trend, J. E.; Poirier, R. J.; Paolucci, D. M.; Maki, S. P.; Lyons, C. S.; Swierczek, M. J. Visual Indicator for Trace Organic Volatiles. *Langmuir* **2010**, 26, 3767-3770.
(5) Budd, P. M.; Elabas, E. S.; Ghanem, B. S.; Makhseed, S.; McKeown, N. B.; Msayib, K. J.; Tattershall, C. E.; Wang, D. Solution-Processed, Organophilic Membrane Derived from a Polymer of Intrinsic Microporosity. *Adv. Mater. (Weinheim, Ger.)* **2004**, 16, 456-459.

(6) Rose, I.; Carta, M.; Malpass-Evans, R.; Ferrari, M.-C.; Bernardo, P.; Clarizia, G.; Jansen, J. C.; McKeown, N. B. Highly Permeable Benzotriptycene-Based Polymer of Intrinsic Microporosity. *ACS Macro Lett.* **2015,** 4, 912-915.
(7) Carta, M.; Malpass-Evans, R.; Croad, M.; Rogan, Y.; Jansen, J. C.; Bernardo, P.; Bazzarelli, F.; McKeown, N. B. An Efficient Polymer Molecular Sieve for Membrane Gas Separations. *Science* **2013,** 339, 303-307.
(8) Gao, L.; Alberto, M.; Gorgojo, P.; Szekely, G.; Budd, P. M. High-Flux PIM-1/PVDF Thin Film Composite Membranes for 1-butanol/Water Pervaporation. *J. Membr. Sci.* **2017**, 529, 207-214.
(9) Adymkanov, S. V.; Yampol'skii, Y. P.; Polyakov, A. M.; Budd, P. M.; Reynolds, K. J.; McKeown, N. B.; Msayib, K. J. Pervaporation of Alcohols Through Highly Permeable PIM-1 Polymer Films. *Polym. Sci. Ser. A* **2008,** 50, 444-450.
(10) Gorgojo, P.; Karan, S.; Wong, H. C.; Jimenez-Solomon, M. F.; Cabral, J. T.; Livingston, A. G. Ultrathin Polymer Films with Intrinsic Microporosity: Anomalous Solvent Permeation and High Flux Membranes. *Adv. Funct. Mater.* **2014**, 24, 4729-4737.
(11) Maffei, A. V.; Budd, P. M.; McKeown, N. B. Adsorption Studies of a Microporous Phthalocyanine Network Polymer. *Langmuir* **2006,** 22, 4225-4229.
(12) Kim, H. J.; Kim, D.-G.; Lee, K.; Baek, Y.; Yoo, Y.; Kim, Y. S.; Kim, B. G.; Lee, J.-C. A Carbonaceous Membrane based on a Polymer of Intrinsic Microporosity (PIM-1) for Water Treatment. *Sci. Rep.* **2016,** 6, 36078.
(13) Satilmis, B.; Budd, P. M.;Uyar, T. Systematic Hydrolysis of PIM-1 and Electrospinning of Hydrolyzed PIM-1 Ultrafine Fibers for an Efficient Removal of Dye from Water. *React. Funct. Polym.* **2017,** 121, 67-75.
(14) Ghanem, B. S.; Msayib, K. J.; McKeown, N. B.; Harris, K. D. M.; Pan, Z.; Budd, P. M.; Butler, A.; Selbie, J.; Book, D.; Walton, A. A Triptycene-Based Polymer of Intrinsic Microposity That Displays Enhanced Surface Area and Hydrogen Adsorption. *Chem. Commun. (Cambridge, U. K.)* **2007,** 0, 67-69.
(15) B., M. N.; Bader, G.; J., M. K.; M., B. P.; E., T. C.; Khalid, M.; Siren, T.; David, B.; W., L. H.; Allan, W. Towards Polymer-Based Hydrogen Storage Materials: Engineering Ultramicroporous Cavities within Polymers of Intrinsic Microporosity. *Angew. Chem. Int. Ed.* **2006,** 45, 1804-1807.
(16) Yuan, S.; Kirklin, S.; Dorney, B.; Liu, D.-J.; Yu, L. Nanoporous Polymers Containing Stereocontorted Cores for Hydrogen Storage. *Macromolecules* **2009,** 42, 1554-1559.
(17) Ward, A. L.; Doris, S. E.; Li, L.; Hughes, M. A.; Qu, X.; Persson, K. A.; Helms, B. A. Materials Genomics Screens for Adaptive Ion Transport Behavior by Redox-Switchable Microporous Polymer Membranes in Lithium–Sulfur Batteries. *ACS Central Science* **2017,** 3, 399-406.
(18) Xia, F.; Pan, M.; Mu, S.; Malpass-Evans, R.; Carta, M.; McKeown, N. B.; Attard, G. A.; Brew, A.; Morgan, D. J.; Marken, F. Polymers of Intrinsic Microporosity in Electrocatalysis: Novel Pore Rigidity Effects and Lamella Palladium Growth. *Electrochim. Acta* **2014,** 128, 3-9.
(19) He, D.; Rauwel, E.; Malpass-Evans, R.; Carta, M.; McKeown, N. B.; Gorle, D. B.; Anbu Kulandainathan, M.; Marken, F. Redox Reactivity at Silver Microparticle—Glassy Carbon Contacts Under a Coating of Polymer of Intrinsic Microporosity (PIM). *J. Solid State Electrochem.* **2017,** 21, 2141-2146.
(20) He, D.; Rong, Y.; Kou, Z.; Mu, S.; Peng, T.; Malpass-Evans, R.; Carta, M.; McKeown, N. B.; Marken, F. Intrinsically Microporous Polymer Slows Down Fuel Cell Catalyst Corrosion. *Electrochem. Commun.* **2015,** 59, 72-76.
(21) Rong, Y.; Malpass-Evans, R.; Carta, M.; McKeown, N. B.; Attard, G. A.; Marken, F. High Density Heterogenisation of Molecular Electrocatalysts in a Rigid Intrinsically Microporous Polymer Host. *Electrochem. Commun.* **2014,** 46, 26-29.
(22) Yang, Z.; Guo, R.; Malpass-Evans, R.; Carta, M.; McKeown, N. B.; Guiver, M. D.; Wu, L.; Xu, T. Highly Conductive Anion-Exchange Membranes from Microporous Tröger's Base Polymers. *Angew. Chem. Int. Ed.* **2016,** 55, 11499-11502.
(23) Madrid, E.; Rong, Y.; Carta, M.; McKeown, N. B.; Malpass-Evans, R.; Attard, G. A.; Clarke, T. J.; Taylor, S. H.; Long, Y.-T.; Marken, F. Metastable Ionic Diodes Derived from an Amine-Based Polymer of Intrinsic Microporosity. *Angew. Chem. Int. Ed.* **2014,** 53, 10751-10754.
(24) Heuchel, M.; Fritsch, D.; Budd, P. M.; McKeown, N. B.; Hofmann, D. Atomistic Packing Model and Free Volume Distribution of a Polymer with Intrinsic Microporosity (PIM-1). *J. Membr. Sci.* **2008,** 318, 84-99.
(25) Konnertz, N.; Ding, Y.; Harrison, W. J.; Budd, P. M.; Schönhals, A.; Böhning, M. Molecular Mobility of the High Performance Membrane Polymer PIM-1 as Investigated by Dielectric Spectroscopy. *ACS Macro Lett.* **2016,** 5, 528-532.
(26) Yin, H.; Chua, Y. Z.; Yang, B.; Schick, C.; Harrison, W. J.; Budd, P. M.; Böhning, M.; Schönhals, A. First Clear-Cut Experimental Evidence of a Glass Transition in a Polymer with Intrinsic Microporosity: PIM-1. *J. Phys. Chem. Lett.* **2018,** 9, 2003-2008.
(27) Freeman, B. D. Basis of Permeability/Selectivity Tradeoff Relations in Polymeric Gas Separation Membranes. *Macromolecules* **1999,** 32, 375-380.
(28) Budd, P. M.; McKeown, N. B.; Fritsch, D. Free Volume and Intrinsic Microporosity in Polymers. *J. Mater. Chem.* **2005,** 15, 1977-1986.
(29) Rose, I.; Bezzu, C. G.; Carta, M.; Comesaña-Gándara, B.; Lasseuguette, E.; Ferrari, M. C.; Bernardo, P.; Clarizia, G.; Fuoco, A.; Jansen, J. C.; Hart, Kyle E.; Liyana-Arachchi, T. P.; Colina, C. M.; McKeown, N. B. Polymer Ultrapermeability from the Inefficient Packing of 2D Chains. *Nat. Mater.* **2017,** 16, 932.
(30) McDermott, A. G.; Budd, P. M.; McKeown, N. B.; Colina, C. M.; Runt, J. Physical Aging of Polymers of Intrinsic Microporosity: a SAXS/WAXS Study. *J. Mater. Chem. A* **2014,** 2, 11742-11752.
(31) Swaidan, R.; Ghanem, B.; Litwiller, E.; Pinnau, I. Physical Aging, Plasticization and Their Effects on Gas Permeation in "Rigid" Polymers of Intrinsic Microporosity. *Macromolecules* **2015,** 48, 6553-6561.
(32) Yin, H.; Chapala, P.; Bermeshev, M.; Schönhals, A.; Böhning, M. Molecular Mobility and Physical Aging of a Highly Permeable Glassy Polynorbornene as Revealed by Dielectric Spectroscopy. *ACS Macro Lett.* **2017,** 6, 813-818.
(33) Yin, H.; Chapala, P.; Bermeshev, M.; Pauw, B. R.; Schönhals, A.; Böhning, M. Influence of Trimethylsilyl Side Groups on the Molecular Mobility and Charge Transport in Highly Permeable Glassy Polynorbornenes. *ACS Applied Polymer Materials* **2019,** 1, 844-855.
(34) Carta, M.; Malpass-Evans, R.; Croad, M.; Rogan, Y.; Lee, M.; Rose, I.; McKeown, N. B. The Synthesis of Microporous Polymers Using Tröger's Base Formation. *Polym. Chem.* **2014,** 5, 5267-5272.
(35) Staiger, C. L.; Pas, S. J.; Hill, A. J.; Cornelius, C. J. Gas Separation, Free Volume Distribution, and Physical Aging of a Highly Microporous Spirobisindane Polymer. *Chem. Mater.* **2008,** 20, 2606-2608.
(36) Cebe, P.; Hu, X.; Kaplan, D. L.; Zhuravlev, E.; Wurm, A.; Arbeiter, D.; Schick, C., Beating the Heat - Fast Scanning Melts Silk Beta Sheet Crystals. *Sci. Rep.* **2013,** 3, 1130.
(37) Zhuravlev, E.; Schick, C. Fast Scanning Power Compensated Differential Scanning Nano-Calorimeter: 1. The Device. *Thermochim. Acta* **2010,** 505, 1-13.
(38) Zhuravlev, E.; Schick, C. Fast Scanning Power Compensated Differential Scanning Nano-Calorimeter: 2. Heat Capacity Analysis. *Thermochim. Acta* **2010,** 505, 14-21.
(39) Adam, G.; Gibbs, J. H. On the Temperature Dependence of Cooperative Relaxation Properties in Glass-Forming Liquids. *J. Chem. Phys.* **1965,** 43, 139–146.
(40) Donth, E. The Glass Transition: Relaxation Dynamics in Liquids and Disordered Materials; Springer: Berlin Germany, 2001.
(41) Cangialosi, D.; Alegría, A.; Colmenero, J. Route to Calculate the Length Scale for the Glass Transition in Polymers. *Phys. Rev. E* **2007,** 76, 011514.

(42) Debenedetti, P. G.; Stillinger, F. H. Supercooled Liquids and the Glass transition. *Nature* **2001,** 410, 259.
(43) Brüning, R.; Samwer, K. Glass Transition on Long Time Scales. *Phys. Rev. B* **1992,** 46, 11318-11322.
(44) Vogel, H. The Law of the Relation Between the Viscosity of Liquids and the Temperature. *Phys. Z.* **1921,** 22, 645.
(45) Fulcher, G. S. Analysis of Recent Measurements of the Viscosity of Glasses. *J. Am. Ceram. Soc.* **1925,** 8 339-355.
(46) Tammann, G.; Hesse, W. Die Abhängigkeit der Viskosität von der Temperatur bei unterkühlten Flüssigkeiten. *Z. Anorg. Allg. Chem.* **1926,** 156, 245-257.
(47) Schönhals, A., Molecular Dynamics in Polymer Model Systems. In Broadband Dielectric Spectroscopy, Kremer, F.; Schönhals, A., Eds. Springer Berlin Heidelberg: Berlin, Heidelberg, 2003; pp 225-293.
(48) Boucher, V.M.; Cangialosi, D.; Alegría, A.; Colmenero, J. Enthalpy recovery in nanometer to micrometer thick polystyrene films. *Macomolecules* **2012**, 45, 5296–5306.
(49) Cangialosi, D.; Alegria, A.; Colmenero, J. Cooling Rate Dependent Glass Transition in Thin Films and in Bulk. In Schick, C.; Mathot, V. (Editors) Fast Scanning Calorimetry (Springer International, Switzerland, **2016**) 403-431.
(50) Martin, J.; Stingelin, N.; Cangialosi, D. Direct calorimetric observation of the rigid amorphous fraction in a semiconducting polymer. J. Phys. *Chem. Lett.* **2018**, 9, 990-995**.**

Table of Contents / Graphical Abstract